Label-free classification of cell types by imaging of cell membrane fluctuations using low-coherent full-field quantitative phase microscopy

LABEL-FREE CLASSIFICATION OF CELL TYPES BY IMAGING OF CELL MEMBRANE FLUCTUATIONS USING LOW-COHERENT FULL-FIELD QUANTITATIVE PHASE MICROSCOPY

Toyohiko Yamauchi[ab], Norikazu Sugiyama[a], Takashi Sakurai[c], Hidenao Iwai[a], Yutaka Yamashita[a]
[a]Hamamatsu Photonics K.K., 5000 Hirakuchi, Hamakita-ku, Hamamatsu, 434-8601 Japan;
[b]Spectroscopy Lab., Massachusetts Institute of Technology, 77 Massachusetts Avenue, Cambridge, MA, 02139 USA;
[c] Photon Medical Research Center, Hamamatsu Univ. School of Medicine, 3600 Handa-yama, Hamamatsu, 431-3192 Japan;

ABSTRACT

Cell membrane motions of living cells are quantitatively measured in nanometer resolution by low-coherent full-field quantitative phase microscopy. Our setup is based on a full-field phase shifting interference microscope with a very low-coherent light source. The reflection mode configuration and the low-coherent illumination make it possible to differentiate the weak reflection light from the cell membrane from the strong reflection from the glass substrate. Two cell populations are quantitatively assessed by the power spectral density of the cell surface motion and show different trends.

Keywords: quantitative phase microscope, cell imaging, plasma membrane

1. INTRODUCTION

Cell morphology and deformability are widely studied biophysical phenomena that have been used to examine the voltage-dependent-motion of a cell membrane [1, 2], assess red blood cells (RBCs) according to their membrane tension [3], and diagnose cancerous/non-cancerous cells by their stiffness [4, 5]. Scanning force microscopy with nanometer scale resolution was commonly used to measure cellular membrane morphology, which is related to cellular viscoelasticity [6, 7]. However, scanning force microscopy inevitably applies force to the cells and requires transversal scanning to obtain a three-dimensional image.

Over the past several years, significant progress has been made in quantitative phase microscopy (QPM), which provides full field information of intrinsic cellular morphology and dynamics [3, 8-11]. Based on a quantitative measurement of the optical wavefront passing through or reflected by living cells, QPM is capable of imaging quantitative morphology. In terms of its feasibility for biological application, quantitative phase microscopy has the advantage that it is free of contrast agents and it does not cause any mechanical damage to a cell. Quantitative phase microscopy was applied to assess the mechanical and dynamic properties of RBCs and showed the difference of membrane motion among many genotypes of RBCs [12].

In order to obtain a precise surface morphology without the effect of the inhomogeneity of intracellular structure, reflection mode (RM) setups of the QPM with a low-coherent (LC) light source are desirable [11, 13, and 14]. Using a configuration probing the light reflected by a cell membrane, our group has shown a full-field (FF) surface topography of a living epithelial cell and its dynamic motion, without any *a priori* information of the cellular refractive index [11, 13].

In this paper, as a first statistical biological study by Low-Coherent Full-Field QPM, we show the assessment of the cell membrane motion in two populations of cultured living cell-lines. One population of cells is a human breast cancer cell line named MCF7 and the other is a rat insulinoma cell line named INS1. The difference of the motility of MCF7 cells and INS1 cells is quantitatively assessed. Our results will show distinctive differences between these two populations by analyzing the power spectral density of cell membrane motion.

Three-Dimensional and Multidimensional Microscopy: Image Acquisition and Processing XVII, edited by Jose-Angel Conchello, Carol J. Cogswell, Tony Wilson, Thomas G. Brown, Proc. of SPIE Vol. 7570, 75700X

2. METHOD

2.1 Reflection mode quantitative phase microscope

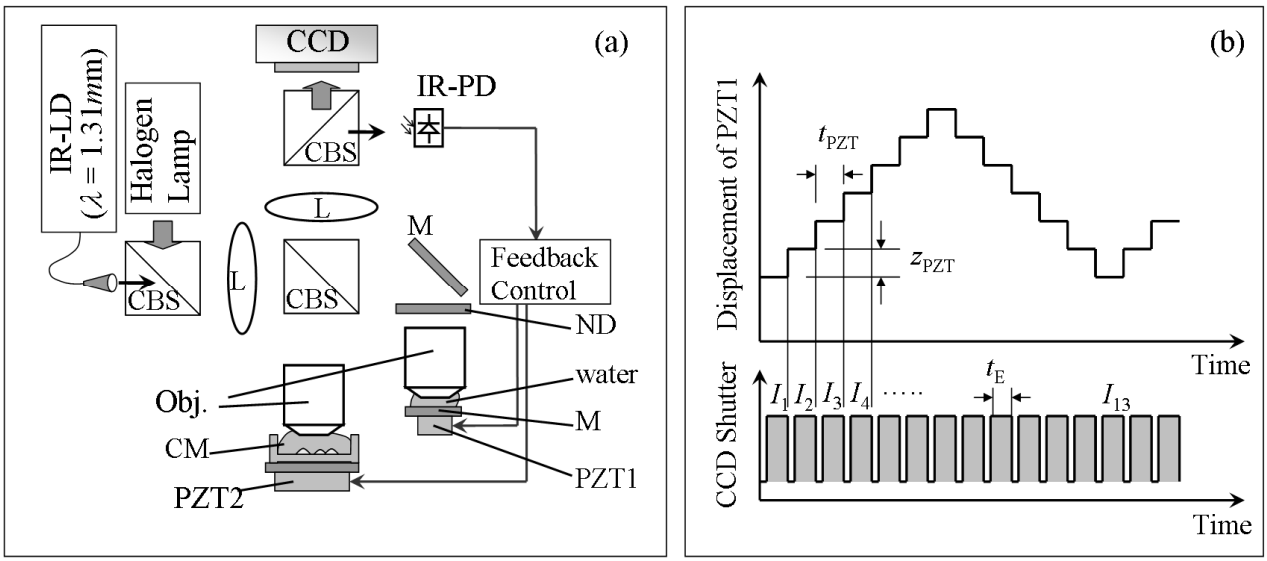

Fig. 1: (a): schematic illustration of setup. IR-LD: infrared laser diode, CBS: cube beam splitter, M: mirror, L: lens, Obj.: objective lens, ND: neutral density filter, PZT: piezoelectric transducer, CCD: charge coupled device camera, CM: culture medium.

(b): schematic diagram of phase shifting and image acquisition.

Our reflection mode quantitative phase microscope is based on phase shifting interference microscopy with precise control of the optical path length [8]. Fig. 1 shows a schematic illustration of the setup. Light emitted from a halogen lamp (center wavelength: 780 nm) passes through a Linnik interferometer provided with two identical water-immersion objective lenses (Nikon, CFI Fluor 60xW, NA = 1.0). The reflected wavefronts from the sample cells and the reference mirror are projected onto the CCD camera (Hamamatsu, C9300-201), and an interference image is obtained.

A series of interferograms is obtained by periodically acquiring interference images while changing the OPD by a step of t_{PZT}, which is a quarter of the center wavelength of the lightsource. The theoretical minimum required number of phase shifting is three, but to reduce the systematic error of the phase estimation and to increase the signal-to-noise ratio, we adopt a seven-point phase shifting algorithm introduced by Hibino et. al, [15]. We show the diagram of the phase shifting in Fig. 1 (b). The phase shifting interval t_{PZT} is 104 msec and one cycle of the raw image acquisition is 1.25 sec (12 times of phase shifting per one cycle). The exposure time t_E of the CCD camera is adjusted so that we get the best intensity without saturation (typically 50~90 msec). The phase of the optical wavefront is calculated by

$$\phi = \tan^{-1}\left(\frac{I_{-3\pi/2} - 3I_{-\pi/2} + 3I_{\pi/2} - I_{3\pi/2}}{2\left(-I_{-\pi} + 2I_0 - I_{\pi}\right)}\right) \tag{1}$$

, where I_ϕ is the raw intensity image with phase shift ϕ. The stepping height of one phase shifting is

$$Z_{PZT} = \frac{1}{4}\cdot\frac{\lambda_c}{2n_w} \tag{2}$$

, where λ_c is the center wavelength of the halogen lamp in air and n_w is the refractive index of water.

The coherence function of the Halogen light measured as a function of the displacement of the sample is shown in Fig. 2., where the coherence length (full width half maxima) is estimated as 1.24 μm in air and 0.93 μm in water. Fig. 3 shows the focal condition on the sample arm. Using PZT1, PZT2 and height adjustment of the objective lenses, the focal plane and the equal-path-length plane, where the optical path length of the reference beam and the sample beam become equal, are matched and set on the middle of the cell under test (typical height: 10μm). Due to the short coherence length of the illumination, only a vertically limited region of the cell membrane around the equal-path-length plane is imaged and obstructive reflection from the glass slide does not contribute to the interference.

The infrared laser diode (IR-LD; emission wavelength = 1.31 μm) is employed to stabilize the optical path difference by a feedback control, as shown in previous papers [8, 13]. The LD light shares the optical path in the interferometer with the halogen light, but is slightly off center in the field of view. The LD light is reflected back from the glass slide under the cell and provides an interference signal on the PD. We show the coherence function of the IR-LD in Fig. 2 as a dashed line. The interference signal of the laser diode is always monitored and the position of the PZT1 is controlled to cancel the mechanical noise in the interferometer. The cells under test are not confluent and the horizontal position of the sample dish is adjusted so the cells in the field of view do not overlap the spot the LD light illuminates. To enhance the interference signal of the IR light, the glass slide under the cell was optically coated to enhance the reflection at 1.3 μm. Note that the glass slide is also anti-reflection coated for the bandwidth of the Halogen lamp.

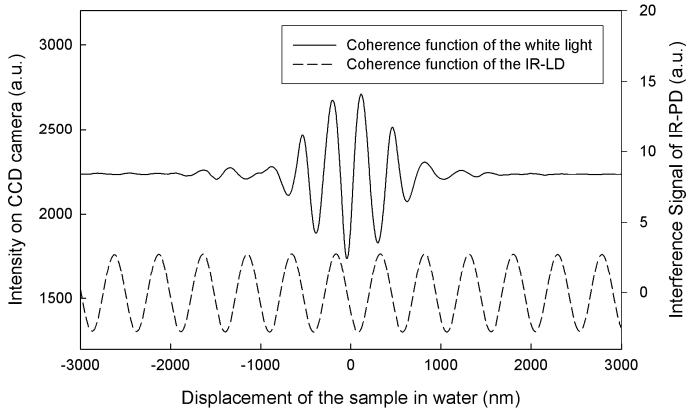

Fig. 2 Coherence function of the Halogen lamp and infrared laser diode

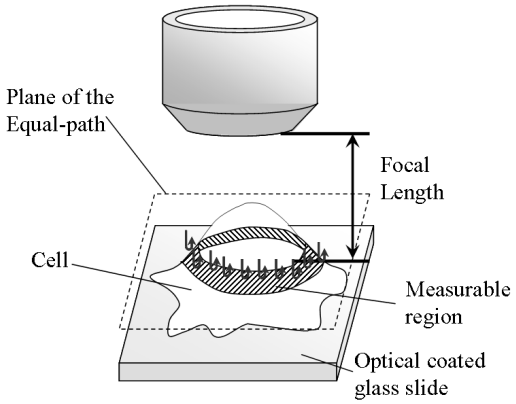

Fig. 3 Focal condition on the sample arm

2.2 Cell preparations

The cell samples are human breast cancer cell line (MCF7) and rat insulinoma cell line (INS1). MCF7 cells are non-excitable cells, while INS1 cells are glucose-dependent insulin-secreting cells. Cells were cultured on the optical-coated

glass slide with RPMI1640 based medium. Immediately before the QPM recording, the medium was exchanged for a HEPES buffered solution containing 130 mM NaCl, 5 mM KCl, 2 mM $CaCl_2$, 1 mM $MgCl_2$, 2.2 mM D-glucose.

3. DATA PROCESSING

This section shows how we quantitatively assessed the surface fluctuation of the cells. Fig. 4 (a) shows an example of a one-shot raw intensity image, where the reference light and the sample light reflected by an intact MCF7 cell surface make concentric interference fringes. Twelve interference images are taken in the manner shown in Fig. 1 (b) in one phase imaging cycle, and the wrapped phase image is calculated by Eq. (2). The wrapped phase image (Fig. 4 (b)) is converted to an unwrapped phase image (Fig. 4 (c)) by Goldstein's phase unwrapping algorithm [16]. The change of the phase $\Delta\phi$ and the change of the height Δh are related by,

$$\Delta h = \frac{\lambda_c}{2n_m} \cdot \frac{\Delta\phi}{2\pi} \tag{3}$$

, where n_m is the refractive index of the culture medium.

We continued the image acquisition for 150 seconds, corresponding to 120 phase imaging cycles, which consists of 1440 raw intensity images. Fig. 5 (a) shows the vertical motion on the points marked as "x" on Fig. 4 (c). To extract parameters representing the characteristics of the motion, we utilize power spectral density (PSD). The PSD at n-th frequency component f (n) is calculated by using a discrete Fourier transform as follows,

$$FFT(n) = \frac{1}{N}\sum_{n=0}^{N-1} \Delta h(m) \cdot \exp\left(-j \cdot 2\pi \frac{m \cdot n}{N}\right) \tag{4}$$

$$PSD(n) = 2N \cdot \Delta t \cdot \left|FFT(n)\right|^2 \tag{5}$$

$$f(n) = n/(N \cdot \Delta t) \quad \text{for } n = 0,1,2 \cdots N/2 \tag{6}$$

, where N is the number of sampling points and Δt is the sampling interval.

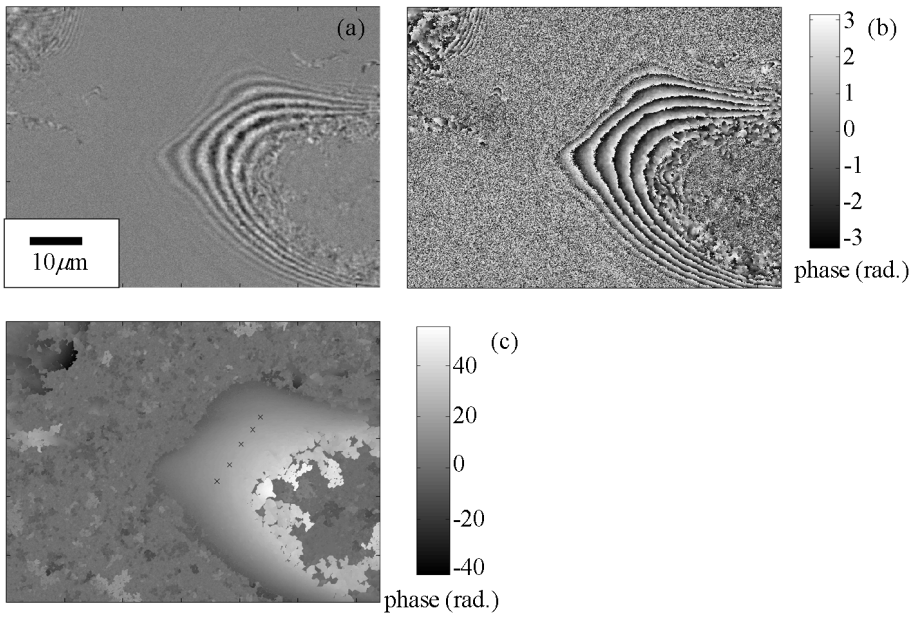

Fig. 4: (a) Interference fringe of the reflection mode imaging of an MCF7 cell, (b) Wrapped phase image of the cell, and (c) Unwrapped phase image of the cell.

We pick up seven or more points, where the phase unwrapping is successful in space and also in time to average the PSD over these points. After averaging, we get the power spectral density shown in the Fig. 5 (b), where a fit curve is also shown by a thick line. We fit Eq. (7) on the averaged PSD using least square fitting.

$$PSD_{fit}(f) = A \cdot f^{s} \tag{7}.$$

As a representative value summarizing the surface fluctuation on the cell, we adopted the slope of the fit curve s and the value of PSD at 0.1 Hz;. The range of the frequency used for the fitting is $0.02Hz \le f \le 0.3Hz$. For example, the fit curve shown in Fig. 5 (b) is $PSD_{fit}(f) = 7.91 \cdot f^{-1.20}$.

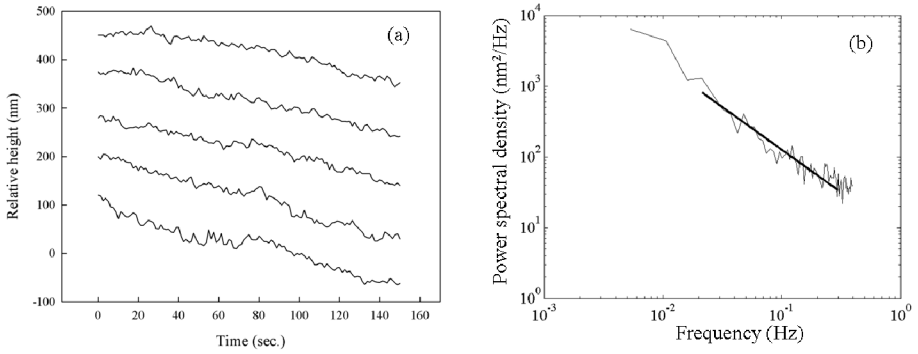

Fig. 5: (a) Vertical motions of the cell surface at the points shown in Fig. 4 (c). (b) Average of the power spectral density of the motions (thin line: raw data, thick line: fit curve).

4. RESULT

4.1 PSD of bead surface

To verify the performance of the setup, we measured the surface of a polystyrene bead. The sample was put on to the optically coated glass slide and immersed in water. Vertical surface motions observed at the points on the bead surface are shown in Fig. 6 (a), and the mean of the PSDs derived from this data are shown in Fig. 6 (b). The vertical motion observed on the bead was below 6.3 nm^2/Hz. The remaining mechanical instability of the setup is expected to be smaller than this fluctuation.

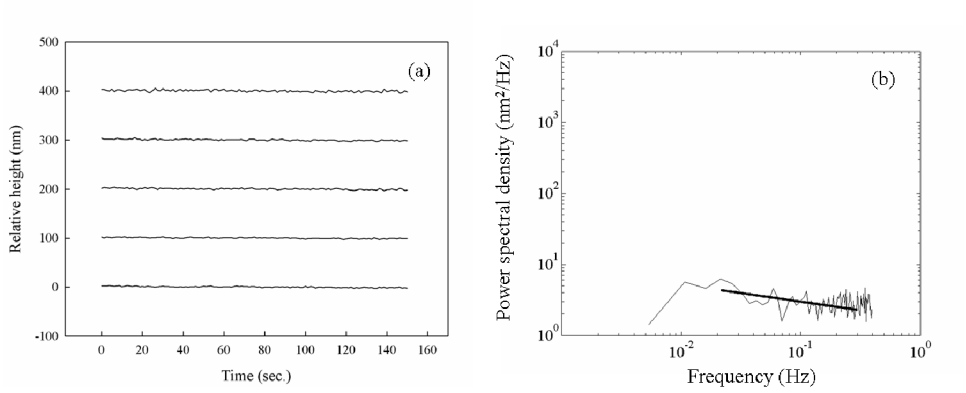

Fig. 6: (a) Vertical motions measured on the surface of the polystyrene bead. (b) Average of the power spectral density of the motions (thin line: raw data, thick line: fit curve).

4.2 PSD of MCF7 cells and INS1 cells

The membrane motion of eleven MCF7 cells and ten INS1 cells were measured. Fig. 7 shows the average of the power spectral density function for each cell population. Fit curves are applied to every cell and the slopes were -1.21 ± 0.37 in MCF7 cells and -1.75 ± 0.25 in INS1 cells (the error is the standard deviation). This result shows that the motility of INS1 cells was higher than the MCF7 cells.

Every cell tested was fixed by paraformaldehyde with a final concentration of 2% and the surface motions of the same cells were measured 5 minutes after the fixation. Fig. 8 shows the average of the power spectral density function after the fixation. The slopes of the fit curves were -0.31 ± 0.21 in MCF7 cells and -0.22 ± 0.22 in INS1 cells. This result implies that after the fixation, the Brownian-motion like fluctuation of the cell membranes were stopped in each cell population and the nature of the fluctuations is more like a white noise. Fig. 9 shows the relation of the slopes before and after the fixations.

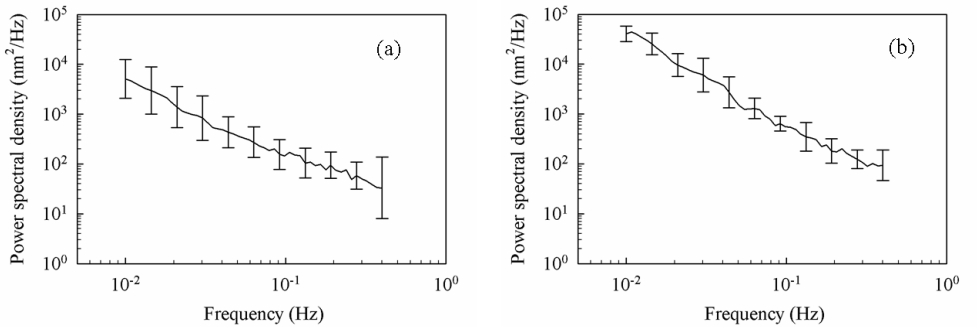

Fig. 7: Average of the PSD. (a) Intact MCF7 cells, (b) Intact INS1 cells. The error bars show the standard deviation of the signal in log scale.

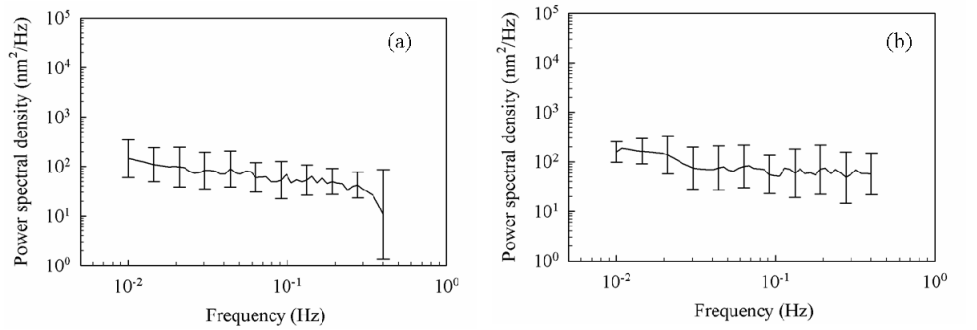

Fig. 8: Average of the PSD. (a) Paraformaldehyde fixed MCF7 cells, (b) Paraformaldehyde fixed INS1 cells. The error bars show the standard deviation of the signal in log scale.

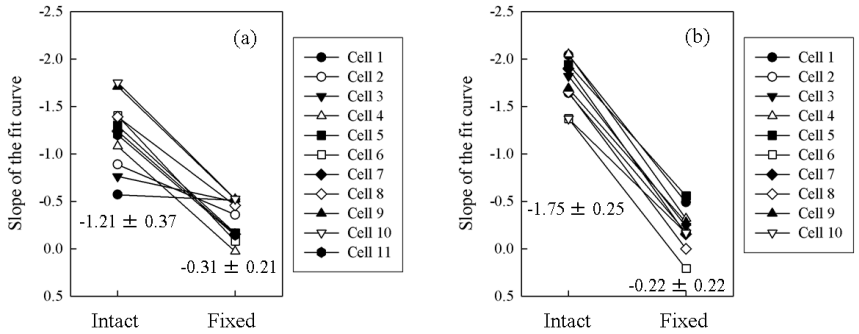

Fig. 9: Slope of the fit curve before and after the fixation. (a) MCF7 cells, (b) INS1 cells.

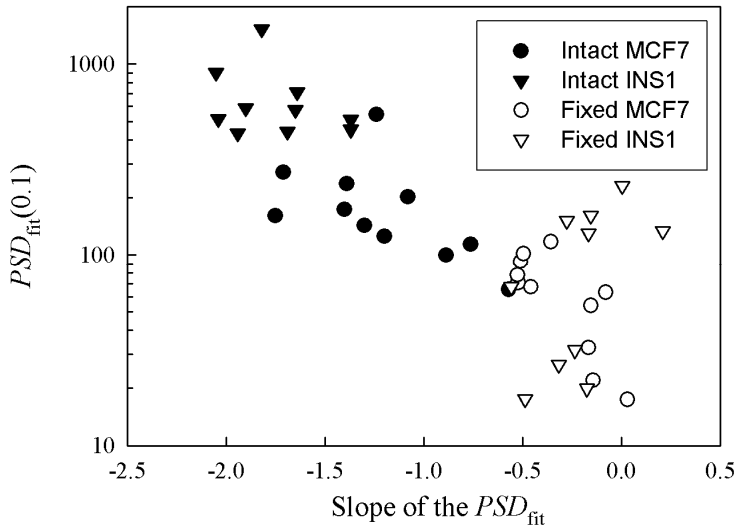

Fig. 10: Scatter plot of the distribution of each cell population.

To summarize the results, we show the distribution of the characteristic parameters of the cell surface motion in Fig. 10. The horizontal axis of Fig. 10 is the slope of the fit curve and the vertical axis is the value of $PSD_{fit}(f)$ at the frequency of $f = 0.1$ Hz.

5. CONCLUSION

It was demonstrated that our Low-Coherent Full-Field Quantitative Phase Microscopy (LC-FF-QPM) is able to stably measure the motion of cell membranes over a long duration. The mechanical noise of the system was below 6.3 nm^2/Hz and this ambiguity is much less than the cell-to-cell variation of the membrane motion. Therefore our system is suitable for quantitatively assessing the intrinsic membrane motion of living cells and it makes it possible to classify different kinds of cells without staining. Since cell-to-cell variation can be caused by the cell cycle, our future works may include the classification of the cell membrane motion for different phases of the cell cycle.

We have found that the power spectral density of the low-frequency cell membrane motion is a good tool to quantify the characteristics of cells. In the low-frequency region (~ 0.4 Hz), the INS1 cells showed a steeper slope in the power spectral density than the MCF7 cells.

Our ultimate goal is the label-free classification of similar cells, like pre-cancer cells and cancer cells of the same organ, at the individual cell level. Since it has been shown that cancerous cells have lower Young's modulus than normal cells [17, 18], cancerous cells are expected to show an intrinsic vibration different from that found in normal cells. We believe that our LC-FF-QPM will be a novel and non-invasive tool to classify cells in terms of their mechanical properties.

ACKNOWLEDGEMENT

The setup of the LC-FF-QPM is based on a collaborative research between Hamamatsu Photonics K.K. and MIT G. R. Harrison Spectroscopy Laboratory. The authors thank Dr. Michael S. Feld, Dr. Ramachandra R. Dasari, Dr. Wonshik Choi, and Dr. Zahid Yaqoob at MIT for their valuable advice.

On the INS1 cell samples, the authors appreciate Dr. H. Mogami, Hamamatsu University School of Medicine.

REFERENCE

[1] P. C. Zhang, A. M. Keleshian, and F. Sachs, “Voltage-induced membrane movement,” Nature 413, 428-432 (2001)

[2] C. Fang-Yen, M. C. Chu, H. S. Seung, R. R. Dasari, and M. S. Feld, “Noncontact measurement of nerve displacement during action potential with a dual-beam low-coherence interferometer,” Opt. Lett. 29, 2028-2030 (2004)

[3] G. Popescu, T. Ikeda, K. Goda, C. A. Best-Popescu, M. Laposata, S. Manley, R. R. Dasari, K. Badizadegan, and M. S. Feld, “Optical measurement of cell membrane tension,” Phys. Rev. Lett. 97, 218101 (2006)

[4] S. Suresh, “Biomechanics and biophysics of cancer cells,” Acta Biomater. 3, 413-438 (2007)

[5] S. E. Cross, Y. S. Jin, J. Rao and J. K. Gimzewski, “Nanomechanical analysis of cells from cancer patients”, Nature Nanotechnology 2, 780-783 (2007)

[6] J. A. Hessler, A. Budor, K. Putchakayala, A. Mecke, D. Rieger, M. M. B. Holl, B. G. Orr, A. Bielinska, J. Beals, and J. Jr. Baker, “Atomic force microscopy study of early morphological changes during apoptosis,” Langmuir. 21, 9280-9286 (2005)

[7] B. Szabó, D. Selmeczi, Z. Környei, E. Madarász, and N. Rozlosnik, “Atomic force microscopy of height fluctuations of fibroblast cells,” Phys. Rev. E. Stat. Nonlin. Soft Matter Phys. 65, 041910 (2002)

[8] H. Iwai, C. Fang-Yen, G. Popescu, A. Wax, K. Badizadegan, R. R. Dasari, and M. S. Feld, “Quantitative phase imaging using actively stabilized phase-shifting low-coherence interferometry,” Opt. Lett. 29, 2399-2401 (2004)

[9] G. Popescu, T. Ikeda, R. R. Dasari, and M. S. Feld, “Diffraction phase microscopy for quantifying cell structure and dynamics,” Opt. Lett. 31, 775-777 (2006)

[10] T. Yamauchi, H Iwai, M. Miwa, and Y. Yamashita, "Measurement of topographic phase image of living cells by white-light phase-shifting microscope with active stabilization of optical path difference," Proc. SPIE 6429, 61 (2007)

[11] T. Yamauchi, H. Iwai, M. Miwa, and Y. Yamashita, "Surface Topography of Cellular Membrane on Nanometer Scale Using White-Light Quantitative Phase Microscope," in Biomedical Optics, OSA Technical Digest (CD) (Optical Society of America, 2008), paper BMD59

[12] G. Popescu, Y.-K. Park, W. Choi, R. R. Dasari, M. S. Feld, and K. Badizadegan, “Imaging red blood cell dynamics by quantitative phase microscopy,” Blood Cells Mol. Dis. 41(1), 10–16 (2008)

[13] T. Yamauchi, H. Iwai, M. Miwa, and Y. Yamashita, “Low-coherent quantitative phase microscope for nanometer-scale measurement of living cells morphology,” Opt. Express 16, 12227-12238 (2008)

[14] Z. Yaqoob, W. Choi, S. Oh, N. Lue, Y. Park, C. Fang-Yen, R. R. Dasari, K. Badizadegan, and M. S. Feld, "Improved phase sensitivity in spectral domain phase microscopy using line-field illumination and self phase-referencing," Opt. Express 17, 10681-10687 (2009)

[15] K. Hibino, B. F. Oreb, D. I. Farrant, and K. G. Larkin, “Phase shifting for nonsinusoidal waveforms with phase-shift errors,” J. Opt. Soc. Am. A 12, 761-768 (1995)

[16] D. C. Ghiglia and M. D. Pritt, “Two-Dimensional phase unwrapping: theory, algorithm, and software”, John Wiley & Sons, Inc., Hoboken, NJ, Chap. 4, (1998)

[17] J. Guck, S. Schinkinger, B. Lincoln, F. Wottawah, S. Ebert, M. Romeyke, D. Lenz, H. M. Erickson, R. Ananthakrishnan, D. Mitchell, J. Kas, S. Ulvick, and C. Bilby, “Optical deformability as an inherent cell marker for testing malignant transformation and metastatic competence,” Biophys. J. 88, 3689-3698 (2005)

[18] M. Lekka, P. Laidler, D. Gil, J. Lekki, Z. Stachura, and A. Z. Hrynkiewicz, ”Elasticity of normal and cancerous human bladder cells studied by scanning force microscopy,” Eur. Biophys. J. 28, 312-316 (1999)